AGU PUBLICATIONS

Geochemistry, Geophysics, Geosystems

RESEARCH ARTICLE
10.1002/2016GC006436

Automated paleomagnetic and rock magnetic data acquisition with an in-line horizontal "2G" system

Tom A. T. Mullender[1], Thomas Frederichs[2], Christian Hilgenfeldt[2], Lennart V. de Groot[1], Karl Fabian[3,4], and Mark J. Dekkers[1]

[1]Paleomagnetic laboratory "Fort Hoofddijk," Department of Earth Sciences, Utrecht University, Utrecht, Netherlands, [2]Research Group Marine Geophysics, Department of Geosciences, University of Bremen, Bremen, Germany, [3]Geological Survey of Norway, Trondheim, Norway, [4]CAGE––Centre for Arctic Gas Hydrate, Environment and Climate, Department of Geology, University of Tromsø, Tromsø, Norway

Key Points:
- A fully automated interface for a horizontal rock magnetometer is described
- Multiple measurement positions enhance paleomagnetic data quality
- Large rock magnetic data sets enable interpretations with high-end algorithms

Supporting Information:
- Supporting Information S1

Correspondence to:
M. J. Dekkers,
m.j.dekkers@uu.nl

Citation:
Mullender, T. A. T., T. Frederichs, C. Hilgenfeldt, L. V. de Groot, K. Fabian, and M. J. Dekkers (2016), Automated paleomagnetic and rock magnetic data acquisition with an in-line horizontal "2G" system, *Geochem. Geophys. Geosyst.*, *17*, 3546–3559, doi:10.1002/2016GC006436.

Received 10 MAY 2016
Accepted 16 AUG 2016
Accepted article online 19 AUG 2016
Published online 5 SEP 2016

Abstract Today's paleomagnetic and magnetic proxy studies involve processing of large sample collections while simultaneously demanding high quality data and high reproducibility. Here we describe a fully automated interface based on a commercial horizontal pass-through "2G" DC-SQUID magnetometer. This system is operational at the universities of Bremen (Germany) and Utrecht (Netherlands) since 1998 and 2006, respectively, while a system is currently being built at NGU Trondheim (Norway). The magnetometers are equipped with "in-line" alternating field (AF) demagnetization, a direct-current bias field coil along the coaxial AF demagnetization coil for the acquisition of anhysteretic remanent magnetization (ARM) and a long pulse-field coil for the acquisition of isothermal remanent magnetization (IRM). Samples are contained in dedicated low magnetization perspex holders that are manipulated by a pneumatic pick-and-place-unit. Upon desire samples can be measured in several positions considerably enhancing data quality in particular for magnetically weak samples. In the Bremen system, the peak of the IRM pulse fields is actively measured which reduces the discrepancy between the set field and the field that is actually applied. Techniques for quantifying and removing gyroremanent overprints and for measuring the viscosity of IRM further extend the range of applications of the system. Typically c. 300 paleomagnetic samples can be AF demagnetized per week (15 levels) in the three-position protocol. The versatility of the system is illustrated by several examples of paleomagnetic and rock magnetic data processing.

1. Introduction

1.1. SQUID Magnetometers for Paleo- and Rock Magnetism

The first described superconducting quantum interference device (SQUID) for rock magnetic measurements was a two-axis system equipped with radio-frequency driven SQUIDs (RF SQUID), each with a single Josephson junction [*Goree and Fuller*, 1976]. Today, the most sensitive magnetometers widely applied for paleomagnetic research have three direct-current biased SQUIDs (DC SQUIDs) as their sensing system, with two Josephson junctions in each SQUID [see *Braginski and Clarke*, 2004]. These DC SQUIDs are biased to operate near the critical currents of their Josephson junctions where quantum interference yields a maximal voltage response to changes in magnetic flux through the SQUID coils. The measurement system is then kept at this most sensitive configuration by means of a flux-locked feedback loop, leading to a very sensitive system with a linear flux-to-voltage response. The output of three sets of superconducting pickup coils around the center of the rock measurement region, are routed to the input signal coupling coils of the SQUID sensors (*Goree and Goodman*, 2003). Such DC SQUID systems are extremely sensitive, enabling measurement of magnetic moments down to $1 \cdot 10^{-12}$ Am^2. A detailed and enjoyable review of the technical background is *Bowles* [2009].

1.2. Automated Systems for Multistep Remanent Magnetization Measurements

Although individual SQUID measurements are performed within less than 1 s, the large number of repeated demagnetization and measurement steps and the related sample movements required for rock and paleomagnetic studies are time-consuming. Stepwise progressive demagnetization of natural or laboratory-induced remanent magnetizations typically involve a substantial number of demagnetization steps, either

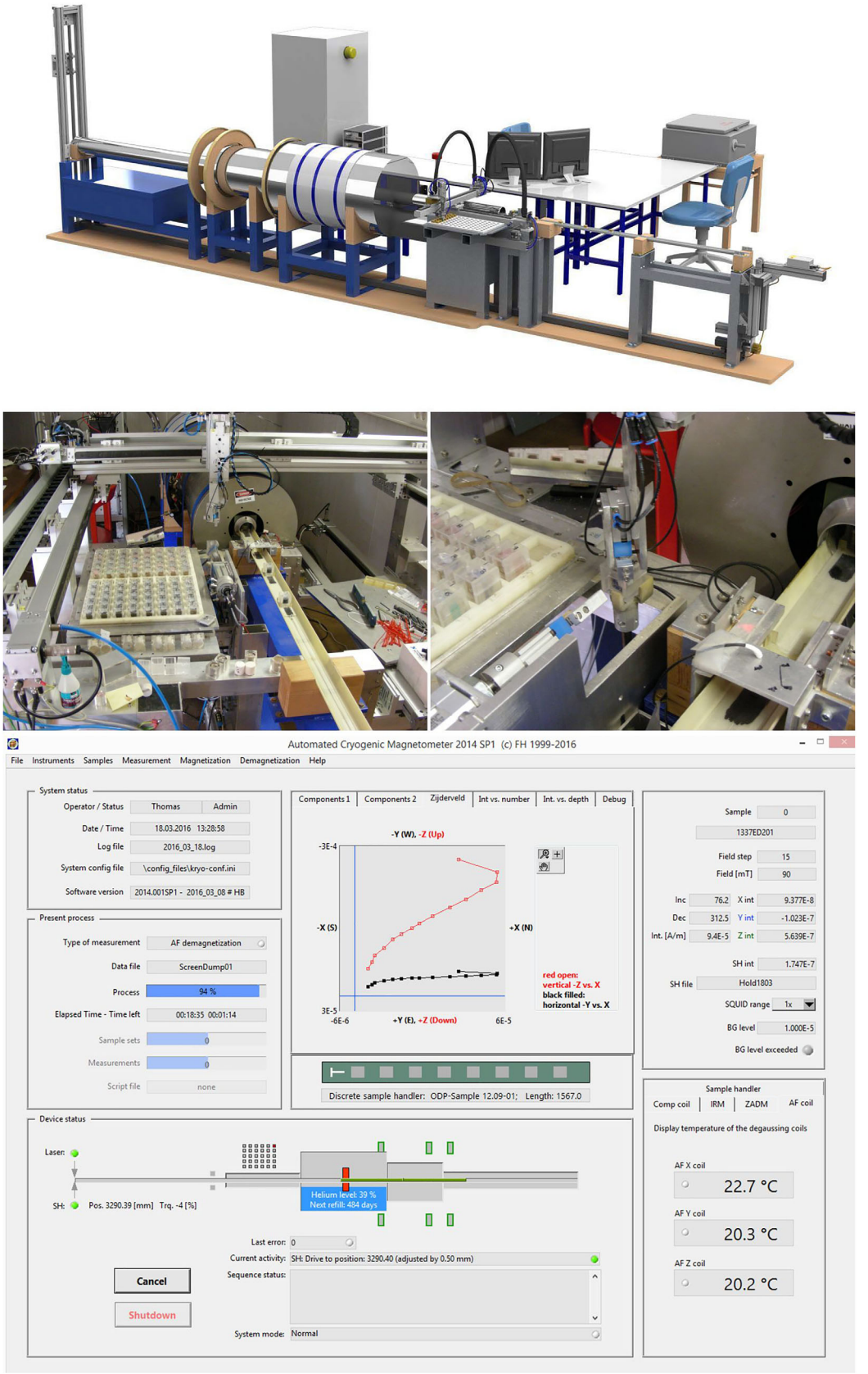
Automated Cryogenic Magnetometer 2014 SP1 (c) FH 1999-2016
File Instruments Samples Measurement Magnetization Demagnetization Help
System status
Operator / Status Thomas Admin
Date / Time 18.03.2016 13:28:58
Log file 2016_03_18.log
System config file \config_files\kryo-conf.ini
Software version 2014.001SP1 - 2016_03_08 # HB
Present process
Type of measurement AF demagnetization
Data file ScreenDump01
Process 94 %
Elapsed Time - Time left 00:18:35 00:01:14
Sample sets 0
Measurements 0
Script file none
Components 1 Components 2 Zijderveld Int vs. number Int. vs. depth Debug
-Y (W), -Z (Up)
-X (S)
+X (N)
+Y (E), +Z (Down)
red open: vertical -Z vs. X
black filled: horizontal -Y vs. X
Discrete sample handler: ODP-Sample 12.09-01; Length: 1567.0
Sample 0
1337ED201
Field step 15
Field [mT] 90
Inc 76.2 X int 9.377E-8
Dec 312.5 Y int -1.023E-7
Int. [A/m] 9.4E-5 Z int 5.639E-7
SH int 1.747E-7
SH file Hold1803
SQUID range 1x
BG level 1.000E-5
BG level exceeded
Sample handler
Comp coil IRM ZADM AF coil
Display temperature of the degaussing coils
AF X coil 22.7 °C
AF Y coil 20.3 °C
AF Z coil 20.2 °C
Device status
Laser:
SH: Pos. 3290.39 [mm] Trq. -4 [%]
Helium level: 39 %
Next refill: 484 days
Last error: 0
Current activity: SH: Drive to position: 3290.40 (adjusted by 0.50 mm)
Sequence status:
Cancel
Shutdown
System mode: Normal

Figure 1.

by alternating fields of increasing strength, or by heating to increasingly elevated temperatures in dedicated field-free furnaces. To reduce operator time and minimize handling differences between samples, several systems have recently been implemented that reach a variable level of automation [e.g., *Frederichs et al*., 2000a; *Kirschvink et al*., 2008, 2015; *Morris et al*., 2009; *Wack and Gilder*, 2012]. Here we report on two systems, based on a common software platform, that allow the fully automated processing of up to 96 samples attached to a horizontal "2G" SQUID magnetometer with in-line alternating field (AF) demagnetization, acquisition of anhysteretic remanent magnetization (ARM) up to 150 (300) mT and acquisition of isothermal remanent magnetization (IRM) up to 700 mT. Measurement and sample handling systems are interfaced with a PC via a LabVIEW® program that interprets the measurement script, controls the instruments and monitors critical variables of the system's state (e.g., demagnetization coil temperature).

A script-driven control software subjects the sample set to any desired sequence of remanence demagnetization or acquisition experiments as defined in a single script file. This ensures error-free sample handling and reproducible data acquisition. In addition, it frees up a considerable amount of precious operator time. The initial system developed by the Marine Geophysics group, Department of Geosciences, Bremen University, Germany [*Frederichs et al*., 2000a, 2000b] has been applied to several magnetometers and improved in various ways. Here we describe the two main systems, operational at the Universities of Utrecht (Netherlands) and Bremen (Germany), and provide examples of the system's performance and indicate potential future developments.

2. Concise Overview of the 2G Magnetometer System

The long-core version of the superconducting rock magnetometer Model 755 HR consists of three orthogonal DC-SQUIDs and three orthogonal coils for alternating field demagnetization. The noise level is lower than $1{\bullet}10^{-12}$ Am^2 which translates into a sample magnetization of 10^{-7} Am^{-1} for standard 10 cm^3 paleomagnetic samples. At the sensing region of the pickup coils of the SQUIDs, and at the center of each of the AF coils, the intensity of the residual field in each direction inside the magnetic shielding is < 25 nT for the Bremen system and even < 5 nT for the Utrecht system. The difference is probably related to the housing of the systems: the Utrecht magnetometer is located in a shielded room while the Bremen magnetometer is not.

The instruments are equipped with an inline pulse magnetizer used for the stepwise acquisition of isothermal remanent magnetization (IRM; cf. (Figure 1, top plot for a photorealistic CAD drawing of the Bremen system). The practical maximum field is 700 mT depending on the bore size of the magnetometer. A DC coil inside the AF coils allows the acquisition of anhysteretic remanent magnetization (ARM) in bias fields up to 0.4 mT. Either individual u-channels or up to eight discrete samples on a tray can be handled. To avoid cross-talking of sample signals, discrete samples are positioned at distances of 20 cm on the sample tray that slides through the bore of the magnetometer (Figure 1, central left plot showing the sample loading/unloading configuration of the Utrecht system). To ensure optimal SQUID performance each unit of the magnetometer system is properly grounded to a dedicated instrumental electric ground. The SQUID electronics are on fast mode. Air is blown through the magnetometer bore to prevent condensation. Air should not be too dry, however, (preferably relative humidity $\sim$50%) otherwise static electricity as a consequence of tray manoeuvering in the magnetometer system severely interferes with its SQUID performance.

2.1. Automation, Hardware Control

To increase the system's efficiency, i.e., the number of samples processed per unit of time, a pneumatic pick-and-place-unit (PAPU) automatically loads and unloads up to 96 discrete samples in sets of eight specimens. For example, the operator could define an initial stepwise alternating field (AF) demagnetization sequence of the NRM, followed by (a combination of) e.g., an ARM acquisition with a user-defined number

Figure 1. (top) Bremen system; photorealistic CAD drawing. (left to right) Counterweight of the position-control system (see also supporting information), long core IRM impulse magnetizer (inside small-diameter mumetal shields), alternating field demagnetization coils (inside intermediate-diameter mumetal shields), the SQUID magnetometer itself (inside large-diameter mumetal shielding), the pick-and-place unit and the facility to load u-channels. Middle panels. Utrecht system. (left) Sample storage tray with pick-and-place unit and the tray that slides through the magnetometer system with a sample spacing of 20 cm to avoid cross-talking between strongly magnetic samples. (right) two-axis rotator enabling positioning of the cubic sample containers upon desire. Lowermost panel. Bremen system. Main screen of LabVIEW® National Instruments-based software controlling the 2G magnetometer with data presentation as component plots, Zijderveld plots, plots of (top middle) magnetic moment versus applied magnetic field, (middle) animated schematic presentation of system components (indicating when active) and(bottom middle and right side) system status information.

of steps, another AF demagnetization, a stepwise IRM acquisition, a single step IRM acquisition in a peak field, and/or an application of a back field by automatically rotating the samples. Lining up several types of these paleo- and rock magnetic measurements in combination with the use of the PAPU makes it possible to operate the magnetometer for up to several days without intervention of the operator. As a rule of thumb, each sample treatment (NRM, ARM or IRM stepwise acquisition or demagnetization) for a set of 96 samples requires approximately 24 h in a single-position protocol. This time period is prolonged in case of the multi-position protocol (Figure 1, central right plot, Utrecht system, the 2-axis rotator to achieve multiple sample positions).

Despite the unchallenged benefits of an automated system, its requirements with respect to the technical reliability are more demanding than those of a manually operated instrument. Mechanical, electrical, and electronic stability are equally essential as the possibility to inform the user about measurement progress, system status, and data quality already during the measurement procedure. The latter is of foremost importance in case of NRM demagnetization, where system problems during demagnetization can lead to the irrevocable loss of potentially invaluable sample data.

To this end the software package was developed in conjunction to improving the hardware, with a focus on safety issues as the instrument operates remotely, i.e., without direct operator control. Specific features are listed below:

1. To avoid erroneous ARM acquisition curves or AF demagnetization behavior it is electronically confirmed whether the programmed AF amplitudes are actually achieved by the instrument. If this is not the case the software shuts down in a controlled way so that measurement can be continued after a manual check. For safety reasons - i.e., to avoid overheating of the coils - a timer is set as soon as the alternating field is being ramped up. The power is automatically cut off after an appropriate period (in seconds/minutes) in case the system would produce an error while the AF coils are powered.
2. Continuous monitoring of the AF coil temperature. Failures in the control electronics of the AF coils could leave the coils switched on for a prolonged time, a definitely undesired situation. This would lead to overheating of the coils which may ruin the coils. Therefore, the temperatures of the AF coils are individually monitored by thermocouples attached to their surfaces. Whenever a coil reaches a critical surface temperature (40°C), further demagnetization (or ARM acquisition) is delayed under software control until the coil has cooled to a safe temperature. This monitoring also prevents overheating as a consequence of repeated demagnetization at high AF levels.
3. Galvanic isolation of all communication paths. This is to reduce the potential effects of a power outage during automated runs (or other uncontrolled electric conditions) which may lead to a chain reaction whereby a damaged component would destroy all the connected electronic devices. As an additional safeguard, and to ensure supply of a stable voltage, an online uninterruptible power supply (UPS) is linked to the SQUID electronics and the computer devices to allow a safe system shut down in case of a power outage.
4. Flux-jump handling. It is well known that under some conditions due to either unusually large magnetization of a sample, rapid tray movement, or electronic failures, the locked-in feedback cycle of the DC SQUID can create flux jumps which lead to erroneous magnetization measurements. These are recognized by background measurements and are corrected by repetition of the measurement. If flux jumps continue to occur (because of too strong samples, mostly during IRM acquisition curves) the samples are unloaded; the measurement sequence obtained so far, is saved so that only meaningful data are being stored.
5. Control of sample holder position during loading, unloading, and sample rotation for multiple position measurements. The original stepper-motor position control appeared not to be sufficiently precise and reproducible adversely affecting the SQUID sensing characteristics [see e.g., *Lascu et al*., 2012]. This issue is solved differently in the Bremen (laser distance meter), Utrecht (optical sensors) and Trondheim systems (webcam based tray positioning), see the respective sections in the supporting information for details.

2.2. Automation, Software Aspects

An in-house developed LabVIEW® National Instruments-based program on a Windows PC connected to a local area network controls all instruments (see Figure 1 lowermost panel for a screenshot of the main

screen during execution of a demagnetization series, Bremen system). The measurement sequence, PAPU commands, magnetometer readings and demagnetization level or remanence acquisition level instructions are scripted via a script in ASCII. This creates maximum flexibility for the user in designing the measurement procedure. Up to 96 specimens can be processed in batches of up to eight; the number of demagnetization levels, ARM or IRM steps is unlimited. If during a measurement procedure certain samples become too strongly magnetic for the magnetometer (e.g., during IRM acquisition) as noticed from instable base line readings, the sequence is terminated and data acquired so far are stored. Too magnetic specimens can be sized down and the sequence can be finalized later without any data loss. Monitoring of the measurement progress is possible in the laboratory but also from remote PCs.

In an automatically generated log file (in ASCII) essentially all system operations are recorded. This enables tracking down causes of (rare) malfunctioning of the instrument. To achieve transparent and reproducible data acquisition raw data are stored immediately after acquisition next to storage in the aforementioned log files. Further, data are stored in individual files after each level of demagnetization or ARM or IRM acquisition, enabling full data recovery when the program would be terminated abruptly. After completion of a measurement sequence evidently data are stored in the desired user-defined format. During the ongoing measurement procedure, it is possible to assess whether the measurement procedure is actually the desired one. To assess the quality of the data obtained, visual presentation of all data in appropriate plots is also available during the measurement. This includes magnetization and demagnetization curves, Zijderveld and component plots, and stereographic plots.

3. Examples

3.1. Alternating Field Demagnetization

The bore of the magnetometer instrument dictates the maximum AF demagnetization level. The Bremen system (42 mm bore) can handle 170 mT peak AF in the "X" and "Y" directions (transversal coils) and 300 mT in the "Z" direction (axial coil). In the Utrecht system (55 mm bore) these maximum values are respectively 140 and 200 mT. There is no active cooling on the AF demagnetization coils. To avoid overheating we practically limit the maximum alternating fields for AF demagnetization to 100 mT; for ARM acquisition (which is along the Z axis) we adhere to 150 mT.

The AF demagnetization is performed by slowly moving the sample tray away from the coils after having been ramped up to the desired demagnetization level, so-called dynamic AF demagnetization. The velocity of the sample tray is programmed as inversely proportional to the peak field of the demagnetization level to ensure optimal data quality. It is possible to perform stationary AF demagnetization. This, however, is considerably more time-consuming. In the so-called ARM test (see section 3.4) the ARM acquisition curve starting from the NRM state in a DC-bias field of 0 μT is actually a single-axis stationary AF demagnetization.

3.2. NRM Demagnetization of Limestones

For optimal demagnetization results specimens are measured in several positions. The effect of the three-position protocol is shown in Figure 2. A cleaner AF demagnetization trajectory of the NRM in a weak (starting NRM $\sim$500•10^{-6} Am^{-1}) limestone is observed for the three-position protocol in comparison to the outcome of each separate position. The example is from Organyà Basin (Spain); it was AF demagnetized after thermal demagnetization up to 150°C to enable a better distinction of the characteristic remanent magnetization (ChRM) component [*van Velzen and Zijderveld*, 1995] (see also Figure 3). The results of the study constrained the Mesozoic rotation of Iberia to the Aptian [*Gong et al*., 2008]. The variability of c. 1–2•10^{-6} Am^{-1} at high AF levels may be due to small variability in magnetic moment of the cube sample holder. Therefore, as usual, interpretation of weak samples should be done with caution. However, the majority of the weak samples processed so far showed unstable demagnetization behavior yielding erratic demagnetization diagrams which preclude meaningful interpretation.

Demagnetization examples from the Donbas fold belt (Ukraine) study of *Meijers et al*. [2010] are shown in Figure 3. The sites were collected to determine new paleomagnetic poles for the late Paleozoic in that region to better constrain the apparent polar wander path of Eurasia for Carboniferous times. The new data which yield slightly higher paleolatitudes than previous data, favor the Pangea B configuration to some extent but do not exclude Pangea A. The Lower Carboniferous sites show a tectonic rotation interpreted to

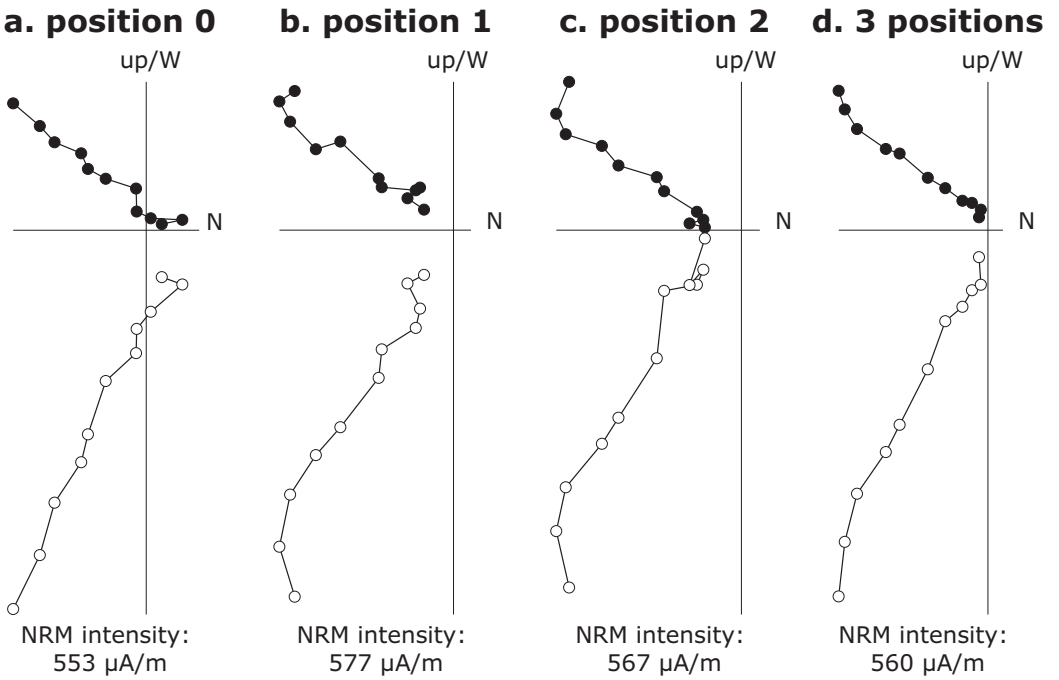

Figure 2. Sample OR39.2A, after correction for the bedding tilt [*Gong et al*., 2008]. Demagnetization levels starting at 20 mT are shown: 20, 25, 30, 35, 40, 50, 60, 70, 80, 90, 100 mT. The ChRM is resolved from 30 mT upward (for unheated samples the ChRM is only resolved from 70 mT upward). Note that demagnetization diagrams of individual positions are somewhat more noisy than the combined 3 position diagram. For the latter the tray contribution is entirely compensated for (Utrecht system).

derive from Mesozoic compressional events. The samples shown here are limestones from the Early Carboniferous: Tournaisian (LC4-76A and LC4-77A), Visean (LC3028A), and Serpukhovian (LC1-37A; regional stage equivalent to the earliest Namurian). The behavior of a particularly weak sample with a starting NRM intensity of $27{\bullet}10^{-6}$ Am^{-1}, LC3-28A) is shown in Figure 3a. Evidently the sample is measured in the three-position protocol. After demagnetization of a laboratory viscous component up to 10 mT and a secondary component up to 30 mT, a meaningful ChRM component is isolated starting at 30 mT. The slight offset from the origin in the Zijderveld diagram is due to a hard magnetic component of the cube sample container. Typical noise of the containers amounts to $1–2{\bullet}10^{-6}$ Am^{-1}; the residual magnetic moment of the containers appears to be directionally stable (see also supporting information Figure S5 and related text). A multicomponent NRM from the same sample collection (LC1-37A) reveals a ChRM from 25 mT upward after removal of a laboratory component and a secondary NRM component (Figure 3b). Many seemingly fresh but incipiently weathered marls and limestones appear to have substantially overlapping characteristic and secondary components demagnetized with AF. If this goes unnoticed, biased ChRM directions may result. The effect of this distracting behavior can be undone by preheating the sample at 150°C followed by AF demagnetization [*van Velzen and Zijderveld*, 1995]. Figure 3c shows the effect: the sample in black (LC4-76A) is not preheated while the first steps of the sample in red (LC4-77A, from the adjacent bed to LC4-76A) are thermal demagnetization steps up to 150°C (room temperature, 90°C, 150°C). The thermally treated sample has a much more distinct ChRM component that is indistinguishable from ChRMs obtained from samples which are thermally demagnetized over the entire temperature range. The ChRM component of the unheated samples is isolated from 60 mT upward while that of the preheated sample is beautifully resolved already from 15 mT upward. Note the difference in inclination (~11°) and declination (~17°) between the two procedures, just AF demagnetization and preheating followed by AF demagnetization. The biased inclinations would lead to too low paleolatitudes while biased declinations would underestimate the amount of vertical axis rotation.

3.3. GRM Correction

The 2G magnetometer system performs static three-axis AF demagnetization, no tumbling is involved. It is well known that certain samples (particularly greigite-bearing samples) are prone to acquire a gyroremanent magnetization (GRM) [cf. *Stephenson*, 1993] during AF demagnetization. For such samples it is advantageous to

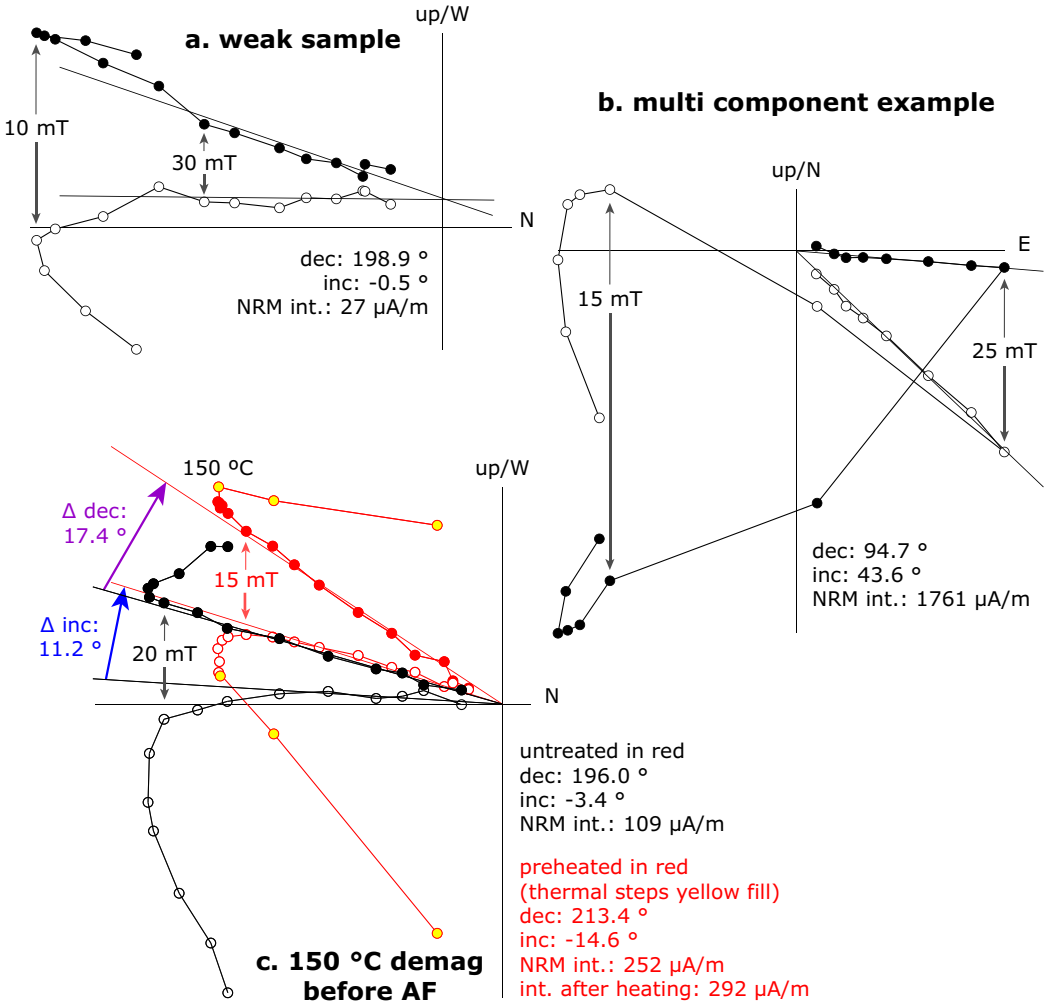

Figure 3. Demagnetization behavior of (a) a weak sample (LC3-28A, this sample was not thermally demagnetized before AF demagnetization), and (b) a multicomponent sample (LC1-37A). (c) The effect of thermal demagnetization up to 150°C on how well the ChRM component is resolved with subsequent AF demagnetization (LC4-76A and LC4-77A). AF demagnetization steps are 0, 3, 5, 8, 10, 15, 20, 25, 30, 40, 50, 60, 70, 80, and 100 mT. Thermal steps before AF (where applicable): 25, 90, and 150°C. All diagrams after tilt correction (Utrecht system).

apply the what is sometimes referred to as the Zijderveld measurement protocol [*Stephenson*, 1993] to remove GRM effects [*Dankers and Zijderveld*, 1981]. This protocol uses only the component parallel to the last demagnetization axis after the sample has been brought into the so-called "cyclic state" [*Dankers and Zijderveld*, 1981; *Stephenson*, 1993]. Theoretical models of GRM [*Stephenson*, 1980a, 1980b, 1983] predict that it is acquired perpendicular to the demagnetization direction. Accordingly, the magnetic vector component along the demagnetization direction should be least affected which forms the basis for GRM correction protocols. In the *Dankers and Zijderveld* [1981] GRM correction procedure the final magnetic vector is assembled from the X component after AF demagnetization along the X axis, the Y component after demagnetization along the Y axis, and the Z component after demagnetization along the Z axis (Figure 4). In numerous samples this procedure almost completely eliminates the biasing magnetic moment generated by GRM effects, a considerable asset since GRM in a samples can be many times stronger than the starting NRM of that sample.

The GRM correction procedure implies five times AF demagnetization at each level rather than three times for the routine AF demagnetization. Also the samples are measured in total three times rather than one time as in the normal procedure. Therefore GRM correction takes a fair amount of additional time and is only enacted from a desired demagnetization level onward: 30 mT when GRM effects become noticeable.

Also in case of an overprint, the developed GRM component can be compensated for by measuring according to the per component protocol which results in a clean ChRM component. The samples in Figure 5 are

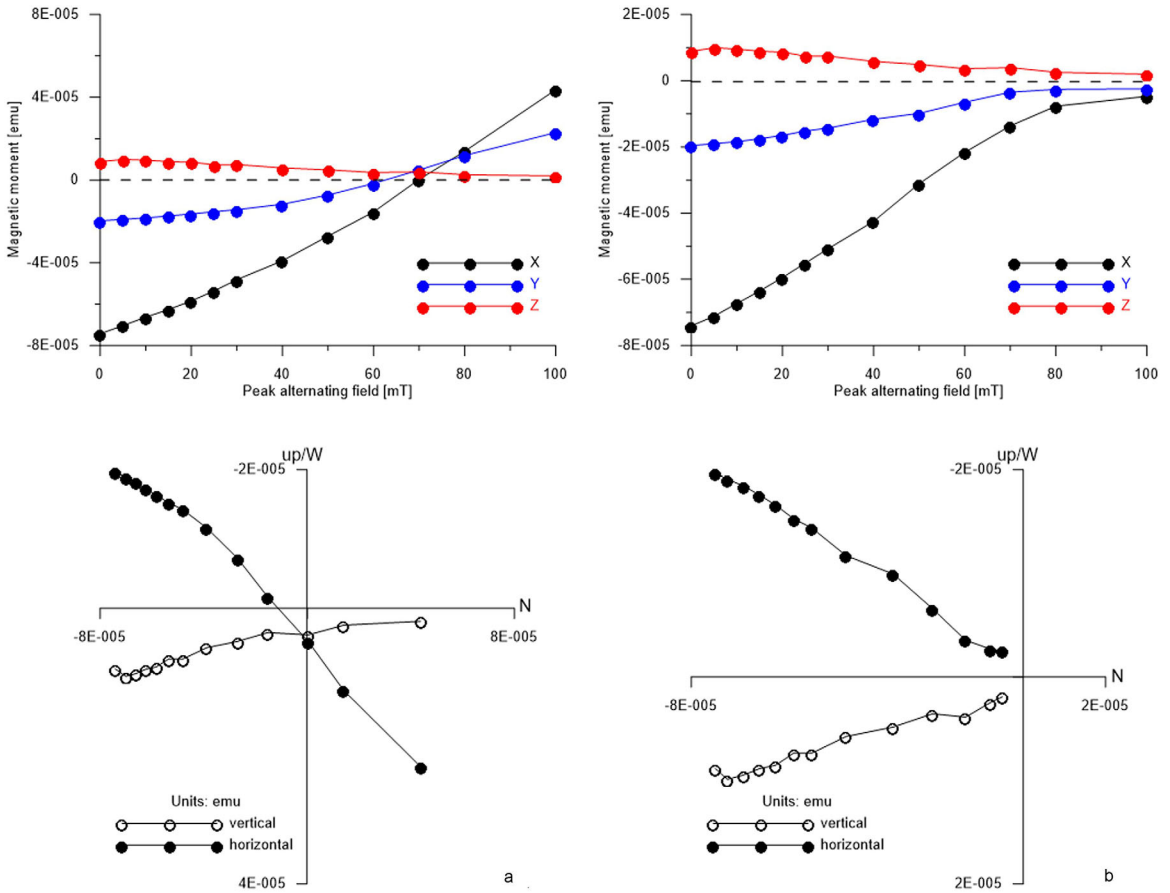

Figure 4. Demagnetization of a greigite bearing sample (GeoB16217-2, 318 cm): (a) results of the normal static three-axis AF demagnetization protocol, i.e., the remaining magnetic moment was determined after all three components had been demagnetized (Bremen system). (b) Results following the GRM correction protocol of *Dankers and Zijderveld* [1981], i.e., measurement of remaining NRM only in the direction of the demagnetizing field applied before (at least taking only that axis into account). Demagnetization sequence was X, Y and then Z. Results for Z direction are identical in both cases since they stem from the same measurement after demagnetization of all three components.

from the Middle Miocene Dinaride Lake System (Serbia and Bosnia & Herzegovina). The magnetostratigraphy of several sections was utilized to date and correlate endemic fauna trends [*de Leeuw et al*., 2010, 2011]. As is well known, fresh water sediments can contain copious amounts of greigite. In some cases (not shown here) GRM development can be that strong that the correction protocol fails [see also e.g., *Hu et al*., 1998].

3.4. Acquisition of Anhysteretic Remanent Magnetization

ARM is considered an analog of TRM and is used as a proxy for the SD fraction in magnetic proxy records. It is, however, a more delicate parameter than often taken for granted. In line with common practice the DC bias field is parallel to the alternating field. Even then ARM can be imparted in two fundamentally different ways: 1) by ramping the alternating field up and down while keeping the sample in place (referred to as stationary method) and 2) the down ramping is achieved by moving the sample away from the alternating field coil (referred to as dynamic method). The latter is unavoidable when u-channels are processed. ARM acquired by the dynamic method is lower than that acquired by the stationary method (Figure 6). Depending on the sample's magnetic properties we found differences in intensity between both methods of up to 40%. The lower ARM in the "dynamic" method is proportional to the field difference of two subsequent half cycles of the alternating field. So for a given DC bias field, the ARM is maximal in the stationary protocol and becomes increasingly lower with increasing velocity of the sample tray in the dynamic protocol. To achieve maximum comparability and to avoid unspecified (!) differences in tray velocity, we always apply the stationary method unless stated otherwise. Only then the DC bias field is fully symmetric. When presenting u-channel data, it is highly recommended to specify the tray velocity that was used during the ARM acquisition together with the DC bias field used.

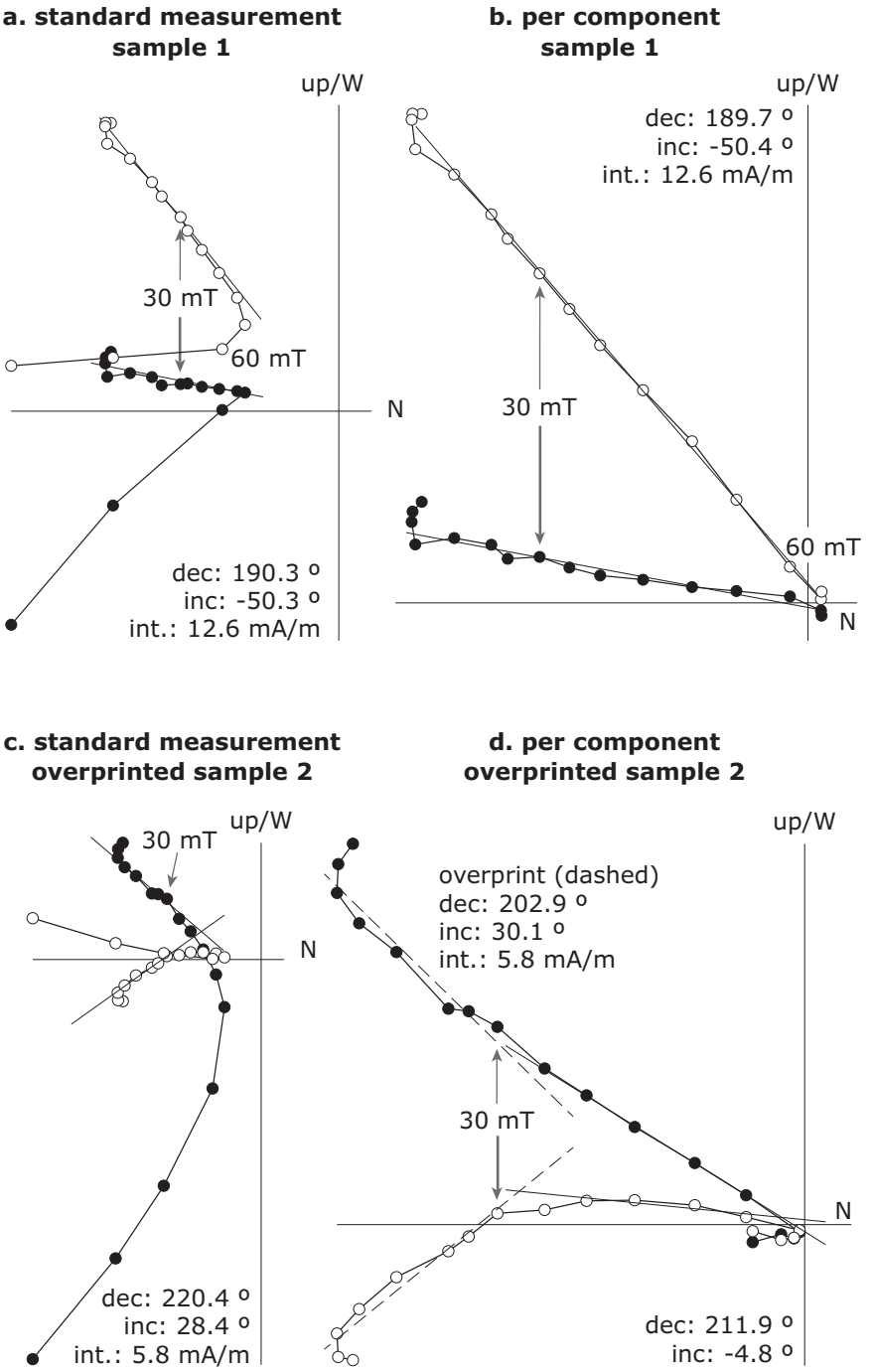

Figure 5. GRM examples from Miocene lake sediments from the Dinarides [*de Leeuw et al*., 2010, 2011] (Utrecht system). (a, b) Sample 44: left AF demagnetization in the standard three-axis treatment (calculated from the per-component data); note the strong GRM developed. (right) the same sample according to the per-component protocol. A clean ChRM is distinguished up to high AF levels. (c, d) Behavior of sample P33.1b. (left) standard protocol with secondary component fitted; (right) per-component protocol.

An application of ARM acquisition curves that currently gains importance is the so-called ARM test used in absolute paleointensity research [*de Groot et al*., 2012]. Because it is rather instrument-intensive it is particularly suited for automated data acquisition. The current application is in conjunction with the multispecimen (MSP) paleointensity protocol [*Dekkers and Böhnel*, 2006; *Fabian and Leonhardt*, 2010]. The ARM test compares the ARM coercivity spectrum of a set of pristine samples to that of a set of sister samples from the same core that has been heated to the temperature at which a MSP experiment will be carried out. From a

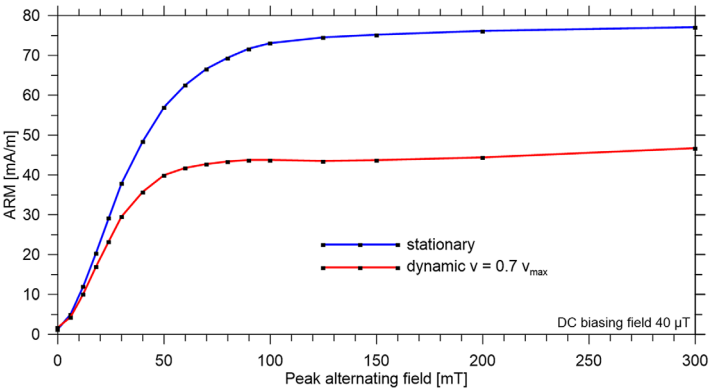

Figure 6. ARM acquisition of a sample applying stationary method (blue) and dynamic method (red) as a function of increasing alternating field (Bremen system).

long drill core at least six specimens are cut which all have the same orientation. Any orientation of the ARM with respect to the NRM will do as long as the orientation is the same for all specimens from a given core. The samples are *not* AF demagnetized before ARM acquisition – this is essential for a meaningful outcome of the test – because static AF demagnetization changes the coercivity spectrum of a sample [*de Groot et al.*, 2012]. Samples are thus given ARMs in increasingly stronger peak AFs starting from the NRM magnetic state or from a partially thermally demagnetized NRM state. Therefore, during the ARM acquisition also the existing NRM is demagnetized simultaneously. It is evident that these two must be separated. By performing ARM acquisition in a 0 μT DC-bias field the NRM demagnetization spectrum is determined. By subtracting these values from the ARM acquisition curve in a given DC-bias field, say 40 μT, the genuine ARM acquisition curve is calculated (Figure 7). This is done for both the pristine, "room temperature" samples and the specimens that were heated before. If their ARM coercivity spectra do not change between room temperature and the desired MSP experiment temperature, the outcome of the MSP experiment (in principle according to the DSC protocol) [*Fabian and Leonhardt*, 2010] is considered meaningful if no thermal alteration occurs during the MSP experiment.

3.5. Acquisition of Isothermal Remanent Magnetization

IRM acquisition curves are commonly used for IRM coercivity component fitting, either based on cumulative log-Gaussian basis functions [e.g., *Kruiver et al.*, 2001] or on skewed generalized Gaussian basis functions [*Egli*, 2003]. Measuring IRM acquisition curves is operator and instrument-intensive; an enormous amount of operator time is saved with automated data acquisition. Examples of IRM acquisition curves with a cumulative log-Gaussian interpretation [*Kruiver et al.*, 2001] are shown in Figure 8. Sample PCOR611 is from the Monti dei Corvi composite section (Italy) [*Hüsing et al.*, 2009]. This section constitutes the basis for the astronomically calibrated geological time scale from ~13 to ~7 Ma because it is beautifully cyclically developed and yields a high-quality magnetostratigraphy retrieved from greigite-bearing strata. In the magnetocyclostratigraphic context demonstrating an early NRM acquisition is essential. The narrow DP of 0.19 log units of the dominant IRM component with a $B_{1/2}$ of 70 mT indicates single-domain particles and points to an important magnetotactic contribution, with a near-primary timing of NRM acquisition formation.

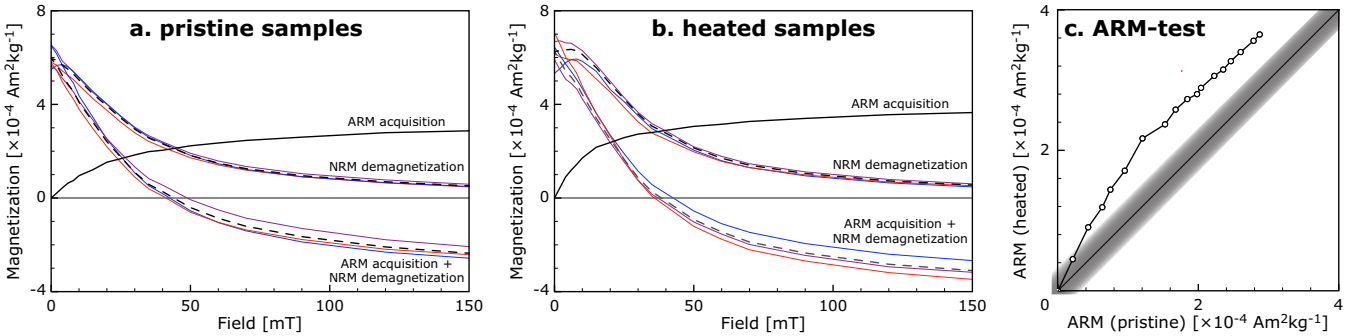

Figure 7. ARM test. (a, b) ARM acquisition resolved from single-axis NRM AF demagnetization (ARM dc bias field 0 μT) and the ARM acquisition in the bias field of 40 μT, referred to as ARM acquisition + NRM demagnetization because NRM is demagnetized simultaneously with the ARM acquisition. (a) pristine samples in the NRM state; (b) samples thermally demagnetized at 220°C, the temperature of the subsequent multispecimen paleointensity experiments. (c) ARM acquisition at room temperature (x axis) plotted against ARM acquisition after heating (y axis). Utrecht system, for further explanation see text.

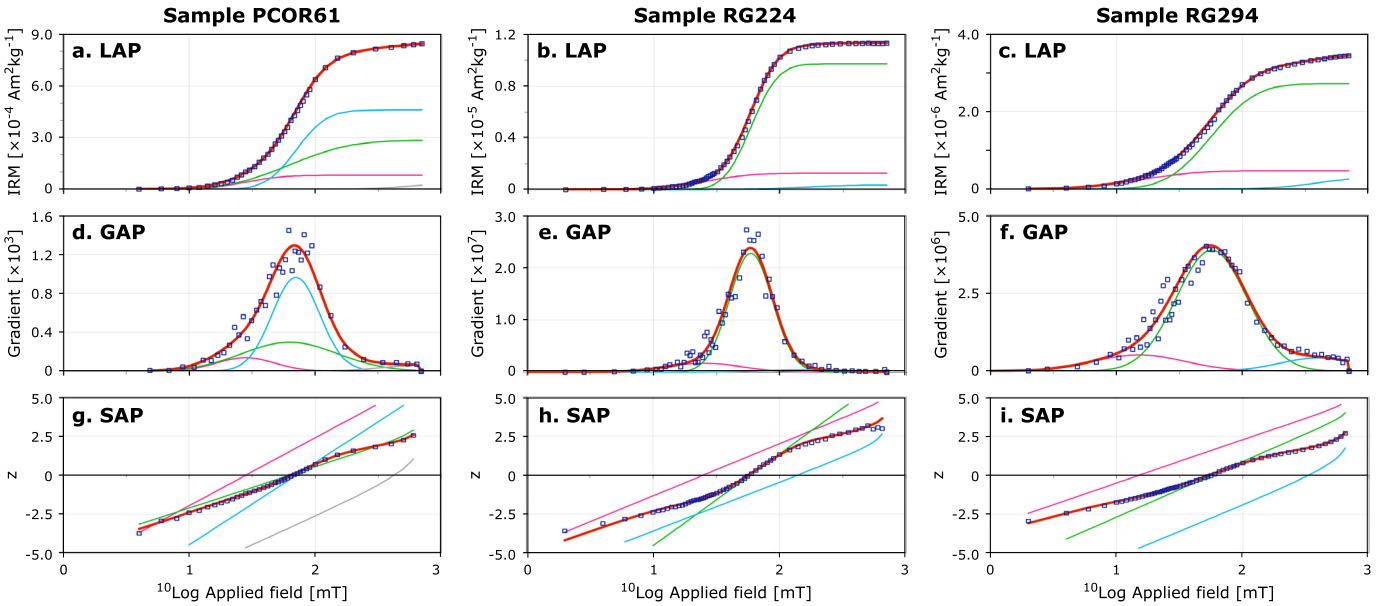

Figure 8. Examples of IRM acquisition curves fitted with the cumulative log-Gaussian approach [*Kruiver et al*., 2001], Utrecht system. Left column: Sample PCOR61 from the Monti dei Corvi section [*Hüsing et al*., 2009]. IRM components are provided from magnetic soft to hard: component 1, $B_{1/2}$ = 28.2 mT, DP = 0.23 (log units), relative amount = 9.3% (extra "component" required to describe the effects of thermal activation that results in a skewed-to-the-left IRM acquisition curve in comparison to a cumulative log-Gaussian IRM acquisition curve [*Egli*, 2004; *Heslop et al*., 2004]; component 2, $B_{1/2}$ = 63.1 mT, DP = 0.38 (log units), relative amount = 32.9% (diagenetic greigite mixed with detrital magnetite which is likely partially oxidized or maghemitized); component 3, $B_{1/2}$ = 70.8 mT, DP = 0.19 (log units), relative amount = 53.4% (magnetotactic greigite); component 4, $B_{1/2}$ = 602.6 mT, DP = 0.28 (log units), relative amount = 4.4% (high coercivity hematite or goethite). For RG224 (central column): component 1, $B_{1/2}$ = 25.1, DP = 0.30, relative amount = 11.3% (thermal activation); component 2, $B_{1/2}$ = 58.9, DP = 0.17, relative amount = 85.5% (magnetotactic with some diagenetic greigite); component 3, $B_{1/2}$ = 141.3, DP = 0.32, relative amount = 3.2% (high coercivity hematite (or goethite)). RG294 (right column): component 1, $B_{1/2}$ = 15.1 mT, DP = 0.36, relative amount = 13.4% (thermal activation); component 2, $B_{1/2}$ = 56.9 mT, DP = 0.28, relative amount = 77.4% (diagenetic greigite and detrital partially oxidized magnetite); component 3, $B_{1/2}$ = 398.1 mT, DP = 0.30, relative amount = 9.1% (high coercivity hematite or goethite).

The two RG samples are from undisturbed Eemian sediments as cored in the "Rutten Gemaal" (Rutten floodgate) oriented core of 28 m long (research core B15F1501 in the Noordoostpolder, the Netherlands) [*Sier et al*., 2015]. The core location is at the position of the lower Rhine delta during the Eemian interglacial. In this Eemian sediments a recording of the Blake Event can be tied to a high-quality pollen record. This enables a precise positioning of the Blake Event in the pollen zonation providing a firm tie point for marine-terrestrial correlation. The lowermost half of the core is dominated by greigite (RG224) while higher up in the core greigite becomes distinctly less prominent as deduced from the wider dispersion as evidenced by a gentler sloping IRM acquisition curve (RG294). While a small dispersion parameter on its own cannot be tied to magnetotactic greigite as firmly as is the case for magnetite, an important magnetotactic contribution is deduced from first-order-reversal-curve diagrams which show a central-ridge signature. This indicates the presence of significant amounts of biogenic magnetic minerals produced by magnetotactic bacteria

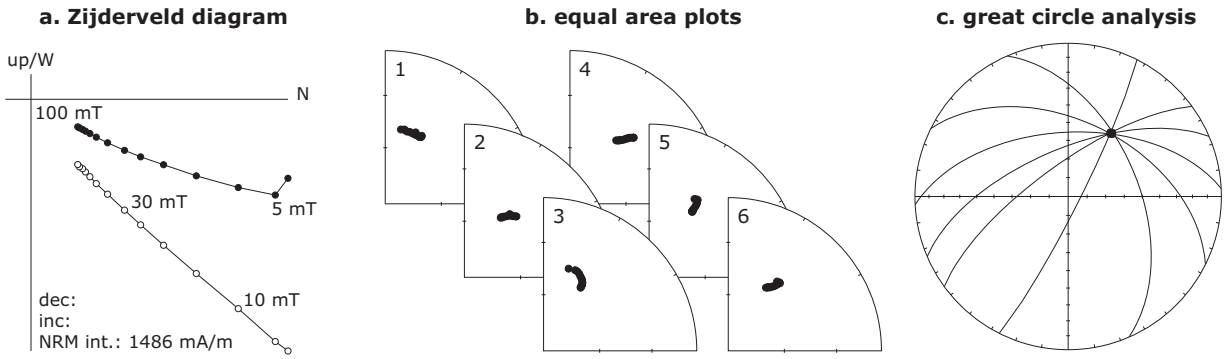

Figure 9. Site AY4 [*van Hinsbergen et al*., 2010]. (a) Example of a demagnetization diagram of a sample affected by lightning. (b) Equal area plots of the demagnetization behavior of six specimens from the site. (c) Great circle analysis; the great circle intersection point is the ChRM direction, indistinguishable from that of nearby sites unaffected by lightning (Utrecht system, in situ coordinates).

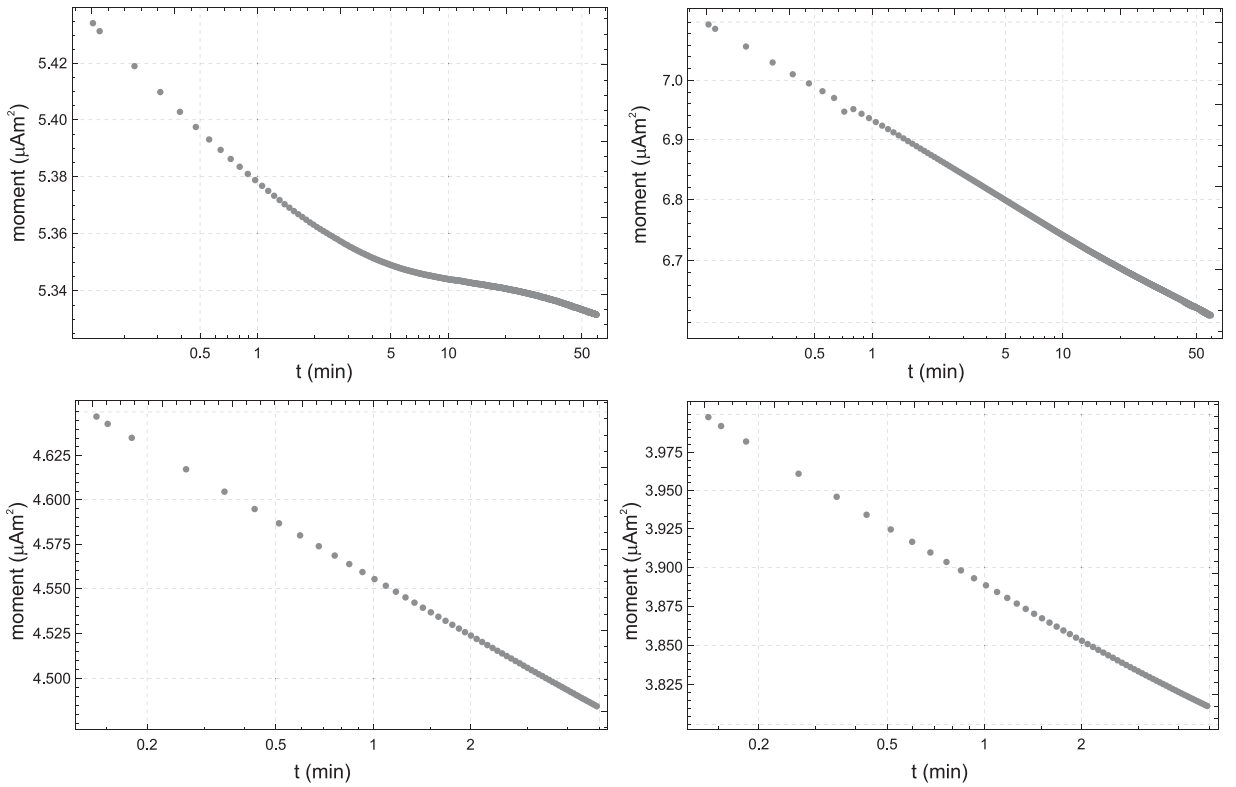

Figure 10. Example measurement of viscous decay in marine sediments (Bremen system). The plots show IRM magnetic moment as a function of log time.

[*Egli et al*., 2010]. Higher up in the core the magnetic assemblage shows a broader switching field distribution (wider DP) compatible with a detrital origin of the dominant magnetic minerals.

End-member modeling of IRM acquisition curves [e.g., *Heslop and Dillon*, 2007; *Gong et al*., 2009; *Just et al*., 2012; *Aben et al*., 2014; *Huang et al*., 2015] requires highly accurate, monotonous IRM acquisition curves, i.e., without negative gradients. Negative gradients play up at the very low and high-field ends of the IRM acquisition curves. Both groups have improved measurement quality in different ways. The Utrecht system has a wider bore than the Bremen system and exact positioning of the sample in the SQUID sensing region is less relevant, taken readings in two measurement positions delivered data of sufficient quality. The Bremen software takes readings at five closely spaced positions with the center position assumed to be optimally placed with respect to the SQUID sensing coils. The highest reading corresponds to the optimum position; potential positioning errors (due to stretching of threading) are traced and corrected for in that way. Further, the actual peak of the pulse field, a more important source of noise, is measured via a shunt circuit rather than calculated, contributing to better data quality (see supporting information for more details). In the Utrecht system small IRM field steps of 1 mT are programmed between 10 and 30 mT, the field region in which the pulse magnetizer showed to be somewhat more noisy ($\pm \sim$1 mT).

An example of a natural IRM is lightning that produces very strong overprints. A lightning strike effects a relatively restricted surface area (a strong strike induces a circular overprint with a diameter of c. 40 m). Therefore the overprint has a different orientation depending on the sample's location in a paleomagnetic site (Figures 9a and 9b). Despite the huge overprints, the primary NRM of a site can be resolved with great circle analysis as shown in the example of site AY4 from the Ayvalik Miocene volcanics (age $\sim$20 Ma) from Western Turkey near to island of Lesbos (Greece) (Figure 9c) [*van Hinsbergen et al*., 2010]. The ChRM direction determined with this approach is the same as those determined by classical vector component analysis for other sites nearby [*van Hinsbergen et al*., 2010]. The study delineated the rotation of the Menderes Core Complex during its exhumation around a pivot point in Western Anatolia in line with metamorphic lineations and other structural geological considerations. The AY sites show a minor clockwise rotation indistinguishable from Eurasia defining the northern limit of the rotation belt.

3.6. IRM Viscosity

Viscosity of IRM is a useful rock magnetic quantity indicating the presence of superparamagnetic particles close to the single-domain threshold in a sample [*Worm*, 1999; *Fabian*, 2003]. Viscosity of IRM (VIRM) is measured by first applying a strong field pulse B_{max} to the sample, then moving it rapidly to the SQUID sensor position, and monitoring the decay of its magnetization over a prescribed length of time with increments dictated by the SQUID reading electronics (~0.2 s per reading) [*Worm*, 1999; *Fabian*, 2003]. In good approximation this decay is represented by the equation

$$M(t) = M_0 - S \log t/t_0 \quad (1)$$

The normalized decay S/M_0 is a quantitative measure of the relative amount of magnetization with decay rate near t_0^{-1}. This is related to the frequency dependent susceptibility [*Worm*, 1999], or, more precisely, to the quadrature susceptibility near the frequency t_0^{-1} [*Shcherbakov and Fabian*, 2005]. Typical measurement times are t_{max} of ~300 s and t_0 of ~10 s. t_0 is limited from below by the time necessary to move the sample from the IRM coil to the SQUID sensor position. Because this initial sample positioning requires an amount of time dependent on the holder's position on the tray of eight sample, the VIRM measurement is performed for a single sample per time, usually the sample closest to the sensors. In unsolidified sediments it may be used to estimate mechanical relaxation processes in a slurry.

4. Conclusion

The robotized system fulfils an important research need: apart from detailed AF demagnetization of the NRM for large amounts of samples, the system enables the acquisition of rock-magnetic data that are increasingly needed for paleomagnetic interpretation. Examples include ARM acquisition curves for the ARM-test in paleointensity research and IRM acquisition curves for magnetic property characterization and end-member modeling. The measurement sequence is always the same, as is the time between acquisition of a laboratory remanence and its measurement. The influence of short-term viscosity effects is minimized and, upon desire, can be evaluated. A significant gain in operator efficiency is achieved: after loading of a batch of samples, the machine runs 24/7. Operators, often students and researchers, can exchange data acquisition time for data interpretation time. Having said this we fully realize that "feel for data quality" is an important aspect of all data and one should never take output as being correct without firm checking. It is recommended to run pilot sequences to optimize the sequence of demagnetization levels for a particular sample collection at hand. The system set-up and program is modular and other types of paleomagnetic and rock magnetic data acquisition can in principle be implemented.

Acknowledgments

The Bremen system was acquired with support of the Deutsche Forschungs Gemeinschaft (DFG). The Utrecht system was acquired with support of the Earth and Life Science branch (ALW) of the Netherlands Science Foundation through their instrument investment program, together with matching funds of the Department of Earth Sciences (Utrecht University). CH is supported by MARUM. KF acknowledges funding through NGU and the Centre of Excellence: Arctic Gas hydrate, Environment and Climate (CAGE) funded by the Norwegian Research Council (grant 223259). This manuscript was finished in loving memory of Tom Mullender who passed away due to a tragic traffic accident in the summer of 2012. He is deeply missed. All data in this contribution are properly cited and referred to in the reference list.

References

Aben, F. M., M. J. Dekkers, R. R. Bakker, D. J. J. van Hinsbergen, W. J. Zachariasse, G. W. Tate, N. McQuarrie, R. Harris, and B. Duffy (2014), Untangling inconsistent magnetic polarity records through an integrated rock magnetic analysis: A case study on Neogene sections in East Timor, *Geochem. Geophys. Geosyst.*, *15*, 2531–2554, doi:10.1002/2014GC005294.

Bowles, J. (2009), SQUID attack!, IRM Q., 19/1, 1, 8–11.

Braginski, A., and J. Clarke (2004), Introduction to The SQUID, in *The SQUID Handbook*, vol. 1, edited by J. Clarke and A. I. Braginski, pp. 251–355, Wiley-VCH Verlag GmbH & Co., Weinheim, Germany.

Dankers, P. H. M., and J. D. A. Zijderveld (1981), Alternating field demagnetization of rocks, and the problem of gyromagnetic remanence, *Earth Planet. Sci. Lett.*, *53*, 89–92.

de Groot, L. V., M. J. Dekkers, and T. A. T. Mullender (2012), Exploring the potential of acquisition curves of the anhysteretic remanent magnetization as a tool to detect subtle magnetic alteration induced by heating, *Phys. Earth Planet. Inter.*, *194-195*, 71–84.

Dekkers, M. J., and H. N. Böhnel (2006), Reliable absolute palaeointensities independent of magnetic domain state, *Earth Planet. Sci. Lett.*, *248*, 508–517.

de Leeuw, A., O. Mandic, A. Vranjkovic, D. Pavelic, M. Harzhauser, W. Krijgsman, and K. F. Kuiper (2010), Chronology and integrated stratigraphy of the Miocene Sinj Basin (Dinaride Lake System, Croatia), *Palaeogeogr. Palaeoclimatol. Palaeoecol.*, *292*, 155–167.

de Leeuw, A., O. Mandic, W. Krijgsman, K. F. Kuiper, and H. Hrvatoviç (2011), A chronostratigraphy for the Dinaride Lake System deposits of the Livno-Tomislavgrad Basin: The rise and fall of a long-lived lacustrine environment, *Stratigraphy*, *8*, 29–43.

Egli, R. (2003), Analysis of the field dependence of remanent magnetization curves, *J. Geophys. Res.*, *108*(B2), 2081, doi:10.1029/2002JB002023.

Egli, R. (2004), Characterisation of individual rock magnetic components by analysis of remanence curves, 2. Fundamental properties of coercivity distribution, *Phys. Chem. Earth*, *29*, 851–867.

Egli, R., A. P. Chen, M. Winklhofer, K. P. Kodama, and C.-S. Horng (2010), Detection of noninteracting single domain particles using first-order reversal curve diagrams, *Geochem., Geophys. Geosyst.*, *11*, Q01Z11, doi:10.1029/2009GC002916.

Fabian, K. (2003), Some additional parameters to estimate domain state from isothermal magnetization measurements, *Earth Planet. Sci. Lett.*, *213*, 337–345.

Fabian, K., and R. Leonhardt (2010), Multiple-specimen absolute paleointensity determination: an optimal protocol including pTRM normalization, domain-state correction, and alteration test, *Earth Planet. Sci. Lett.*, *297*, 84–94.
Frederichs, T., C. Hilgenfeldt, and K. Fabian (2000a), A modified version of the 2G cryogenic magnetometer, *Terra Nostra*, *2000/10*, 41–43.
Frederichs, T., K. Fabian, C. Hilgenfeldt, and A. M. Schmidt (2000b), Experiences with a 2G cryogenic magnetometer, *Geophys. Res. Abstr.*, *2*, 183.
Gong, Z., C. G. Langereis, and T. A. T. Mullender (2008), The rotation of Iberia during the Aptian and the opening of the Bay of Biscay, *Earth Planet. Sci. Lett.*, *273*, 80–93.
Gong, Z., M. J. Dekkers, D. Heslop, and T. A. T. Mullender (2009), End-member modelling of isothermal magnetization (IRM) acquisition curves: A novel approach to diagnose remagnetization, *Geophys. J. Int.*, *178*, 693–701.
Goree, W. S., and M. Fuller (1976), Magnetometers using R.F.-driven squids and their applications in rock magnetism and paleomagnetism, *Rev. Geophys.*, *14*, 591–608.
Goree, W. S., and W. Goodman (2003), 755R Manual, WSGI, Mountain View, Calif. [Available at http://www.wsgi.us/WSGI/MANUALS_files/Cryo_manual_July2003_1.pdf.]
Heslop, D., and M. Dillon (2007), Unmixing magnetic remanence curves without a priori knowledge, *Geophys. J. Int.*, *170*, 556–566.
Heslop, D., G. McIntosh, and M. J. Dekkers (2004), Using time- and temperature-dependent Preisach models to investigate the limitations of modelling isothermal remanent magnetization acquisition curves with cumulative log Gaussian functions, *Geophys. J. Int.*, *157*, 55–63.
Hu, S., E. Appel, V. Hofmann, W. W. Schmahl, and S. Wang (1998), Gyromagnetic remanence acquired by greigite (Fe3S4) during static three-axis alternating field demagnetization, *Geophys. J. Int.*, *134*, 831–842.
Huang, W., et al. (2015), Can a primary paleolatitude be retrieved from partially remagnetized Eocene volcanics in the Nanmulin Basin (Southern Tibet) to date the India-Asia collision?, *J. Geophys. Res. Solid Earth*, *120*, 42–66, doi:10.1002/2014JB011599.
Hüsing, S. K., M. J. Dekkers, C. Franke, and W. Krijgsman (2009), The Tortonian reference section at Monte dei Corvi (Italy): Evidence for early remanence acquisition in greigite-bearing sediments, *Geophys. J. Int.*, *179*, 125–143.
Just, J., M. J. Dekkers, T. von Dobeneck, A. van Hoesel, and T. Bickert (2012), Signatures and significance of aeolian, fluvial, bacterial and diagenetic magnetic mineral fractions in Late Quaternary marine sediments off Gambia, NW Africa, *Geochem. Geophys. Geosyst.*, *13*, Q0AO02, doi:10.1029/2012GC004146.
Kirschvink, J. L., R. E. Kopp, T. D. Raub, C. T. Baumgartner, and J. W. Holt (2008), Rapid, precise, and high-sensitivity acquisition of paleomagnetic and rock-magnetic data: Development of a low-noise automatic sample changing system for superconducting rock magnetometers, *Geochem. Geophys., Geosyst.*, *9*, Q05Y01, doi:10.1029/2007GC001856.
Kirschvink, J. L., Y. Isozaki, H. Shibuya, Y.-I. Otofuji, T. D. Raub, I. A. Hilburn, T. Kasuya, M. Yokoyama, and M. Bonifacie (2015), Challenging the sensitivity limits of paleomagnetism: Magnetostratigraphy of weakly magnetized Guadalupian–Lopingian (Permian) limestone from Kyushu, Japan, *Palaeogeogr. Palaeoclimatol. Palaeoecol.*, *418*, 75–89.
Kruiver, P. P., M. J. Dekkers, and D. Heslop (2001), Quantification of magnetic coercivity components by the analysis of acquisition curves of isothermal remanent magnetisation, *Earth Planet. Sci. Lett.*, *189*, 269–276.
Lascu, I., M. Jackson, and P. Solheid (2012), Beyond u-channels––Improving the deconvolution of u-channel magnetometer data for non-standard sample geometries, *IRM Quarterly*, *22*(3), 8–11.
Meijers, M. J. M., M. F. Hamers, D. J. J. van Hinsbergen, D. G. van der Meer, A. Kitchka, C. G. Langereis, and R. A. Stephenson (2010), New late Paleozoic paleopoles from the Donbas Foldbelt (Ukraine): Implications for the Pangea A vs. B controversy, *Earth Planet. Sci. Lett.*, *297*, 18–33.
Morris, E. R., W. Schillinger, R. S. Coe, C. J. Pluhar, and N. A. Jarboe (2009), Automating the 2G superconducting rock magnetometer for single-solenoid alternating field demagnetization, *Geochem. Geophys. Geosyst.*, *10*, Q05Y05, doi:10.1029/2008GC002289.
Shcherbakov, V. P., and K. Fabian (2005), On the determination of magnetic grain-size distributions of superparamagnetic particle ensembles using the frequency dependence of susceptibility at different temperatures, *Geophys. J. Int.*, *162*, 736–746.
Sier, M. J., J. Peeters, M. J. Dekkers, J. M. S. Paré, L. Chang, F. S. Busschers, K. M. Cohen, J. Wallinga, F. P. M. Bunnik, and W. Roebroeks (2015), The Blake Event recorded near the Eemian Type locality––A diachronic onset of the Eemian in Europe, *Q. Geochronol.*, *28*, 12–28.
Stephenson, A. (1980a), A gyroremanent magnetization in anisotropic magnetic material, *Nature*, *284*, 49–51.
Stephenson, A. (1980b), Rotational remanent magnetization and the torque exerted on a rotating rock in an alternating magnetic field, *Geophys. J. R. Astron. Soc.*, *62*, 113–132.
Stephenson, A. (1983), Changes in direction of the remanence of rocks produced by stationary alternating field demagnetization, *Geophys. J. R. Astron. Soc.*, *73*, 213- 239.
Stephenson, A. (1993), 3-axis static alternating field demagnetization of rocks and the identification of natural remanent magnetization, gyroremanent magnetization and anisotropy, *J. Geophys. Res.*, *98*, 373–381.
van Hinsbergen, D. J. J., M. J. Dekkers, E. Bozkurt, and M. Koopman (2010), Exhumation with a twist: Paleomagnetic constraints on the evolution of the Menderes metamorphic core complex, western Turkey, *Tectonics*, *29*, TC3009, doi:10.1029/2009TC002596.
van Velzen, A. J., and J. D. A. Zijderveld (1995), Effects of weathering on single domain magnetite in early Pliocene marls, *Geophys. J. Int.*, *121*, 267–278.
Wack, M. R., and S. A. Gilder (2012), The SushiBar: An automated system for paleomagnetic investigations, *Geochem. Geophys. Geosyst.*, *13*, Q12Z38, doi:10.1029/2011GC003985.
Worm, H.-U. (1999), Time-dependent IRM: A new technique for magnetic granulometry, *Geophys. Res. Lett.*, *26*, 2557–2560.